

AD-A268 391



2

02/11/93

Atomic-Scale Friction Measurements Using Friction Force Microscopy

Part I - General Principles and New Measurement Techniques

N00014-93-I-0067

Ju-Ai Ruan and Bharat Bhushan (Fellow ASME)

Computer Microtribology and Contamination Laboratory

Department of Mechanical Engineering

The Ohio State University

Columbus, Ohio 43210-1107

DTIC
ELECTE
AUG 20 1993
S A D

Abstract

Friction force measurements using modified atomic force microscopy, called here Friction Force Microscopy (FFM), are becoming increasingly important in the understanding of fundamental mechanisms of friction, wear, and lubrication, and to study interfacial phenomenon in micro- and nanostructures used in magnetic storage systems and Microelectromechanical Systems (MEMS). A review of existing designs of FFMs and methods of friction force measurements is presented. In terms of friction force measurements, there are important issues related to the basic operation and calibration of these instruments which have not been fully studied. A new method of measuring friction force using a commercial FFM and a calibration procedure for conversion of measured data to normal and friction forces are presented. Atomic-scale friction data of selected materials are presented and discussed in light of macro-friction measurements.

This document has been approved
for public release and sale; its
distribution is unlimited.

93-18784



93-18784

49,45

1. Introduction:

Scanning Tunneling Microscope (STM) developed by Binnig et al. (1982) is the first instrument capable of directly obtaining three dimensional (3D) images of solid surfaces with atomic resolution. In the STM, a tunneling current is sensed between a conducting solid and a sharp metal tip (Melmed, 1991) held about 0.3-1 nm above the solid surface with an operating voltage of 2 mV to 2V. Because the current increases by approximately a factor of 10 for each 0.1 nm the tip is brought closer to the surface, the tunneling current (micro to nano amperes) is a very sensitive measure of the tip-surface distance. To image a sample surface, two piezoelectric drivers raster the tip parallel to the plane of the sample. A feedback loop drives a third piezoelectric element perpendicular to the sample to adjust the tip position to keep the current or tip-surface separation constant. The tip position gives a 3D image of the sample surface.

Based on their earlier design of STM, Binnig et al. (1986) developed an Atomic Force Microscope (AFM) to measure ultrasmall forces (less than 1 μ N) present between the AFM tip surface and a sample surface. They measured these small forces by measuring the motion of a cantilever beam having an ultrasmall mass. STM requires that the surface to be measured be electrically conductive, however, AFM is capable of investigating surfaces of both conductors and insulators on an atomic scale if suitable techniques for measurement of cantilever motion are used. In the operation of the high resolution AFM, the sample is scanned instead of the tip as in STM, because the AFM measures the relative displacement between the cantilever surface and reference surface and any cantilever movement would add vibrations.

For imaging of surfaces, AFMs can be thought of as a nanometer scale profilers. A sharp tip at the end of a cantilever is brought within atomic dimensions of a sample surface by moving the sample with piezoelectric transducers. The atoms at the end of the tip experience a repulsive force due to electronic orbital overlap with the atoms in the surface. The force acting on the tip causes a lever deflection which is measured by various techniques such as laser interferometry (Mate et

1
THE SURFACE INSPECTED 1

DIS1
A-1
SPECIAL
or
odes

al., 1987; Erlandsson et al., 1988), Fig.1. The deflection can be measured to within ± 0.02 nm, so for a typical lever force constant of 10 N/m a force as low as 0.2 nN (corresponding normal pressure ~ 1 MPa for a tip radius of about 50 nm) could be detected. This operational mode is referred to as "repulsive mode". An alternative is to use "attractive force imaging", in which the tip is brought in close proximity (within a few nm) to, and not in contact with the sample. Although in this technique the normal pressure exerted at the interface is zero (desirable to avoid any surface deformation), it has poorer resolution. In either mode, surface topography is generated by laterally scanning the sample under the tip while simultaneously measuring the separation-dependent force or force gradient (derivative) between the tip and the surface. The force gradient is obtained by vibrating the cantilever and measuring the shift of resonance frequency of the lever. To obtain topographic information, the interaction force is either recorded directly, or used as the control parameter for a feedback circuit that maintains the force or force derivative at a constant value. With AFM operated in the repulsive mode, topographic images with a vertical resolution of less than 0.1 nm (as low as 0.01 nm) and a lateral resolution of about 0.2 nm have been obtained (Albrecht and Quate, 1987; Marti et al., 1987; Meyer and Amer, 1990a). An important property of AFM is its ability to go beyond topographic measurements and investigate different phenomena associated with forces, such as magnetism (magnetic force measurements including its application for magnetic recording), electrostatic attraction, chemical interaction, and various friction, wear, indentation, and lubrication studies (for example, Martin and Wickramasinghe, 1987; Bhushan, 1990; Blackman et al., 1990; Schonenberger and Alvarado, 1990; Bhushan and Blackman, 1991; Grütter et al., 1991; Maivald et al., 1991; Manne et al., 1991; Ohkubo et al., 1991; Kaneko and Enomoto, 1992; O'Shea Welland, 1992; Bhushan, 1993; Ruan and Bhushan, 1993). In fact, the advent of AFM and its derivatives has led to the development of a new field of microtribology which relates to studies of friction, wear and lubrication on an atomic scale. It has attracted numerous physicists and chemists to this field.

Mate et al. (1987) were first to modify an AFM in order to measure both normal and friction forces and this instrument is generally called "Friction Force Microscope (FFM)", or "Lateral Force Microscope" (LFM) or "Scanning Force Microscope" (SFM). They measured atomic-scale friction of a tungsten tip sliding on a basal plane of a single grain of highly-oriented pyrolytic graphite (HOPG). Since then several research groups have developed various designs of FFMs. There are also a number of manufacturers who produce commercial AFM/FFM instruments with scanning length ranging from about 0.7 μm (for atomic resolution) to about 100 μm or larger (such as Digital Instruments, Santa Barbara, CA and Park Scientific Instruments, Mountain View, CA). In terms of friction force measurement, there are some important issues related to the basic operation and the calibration of these instruments that have not been fully studied.

In this paper, we present a brief review of existing designs of FFMs. We then describe in more detail a new method of measuring friction force using a commercial AFM/FFM and a calibration procedure for conversion of measured cantilever deflection data to normal and friction forces. Atomic-scale friction data of selected materials are also presented and discussed.

2. A Review of Atomic-Scale Friction Measurement Techniques.

The key component in AFM and FFM is the sensor for measuring the force on the tip due to its interaction with the sample. We need a lever (which consists of the tip) with low stiffness for high vertical and lateral resolutions at small forces (0.1 nN or lower) but at the same time a high resonant frequency (about 5 to 20 kHz) in order to minimize the sensitivity to vibrational noise from the building near 100 Hz. This requires a spring with extremely low stiffness (about 10 to 10^3 N/m) as well as low mass (on the order of 1 nN). The force on the tip due to its interaction with the sample is sensed by detecting the deflection of the compliant lever with a known spring constant. This lever deflection (displacement smaller than 0.1 nm) has been measured by detecting tunneling current similar to that used in STM (Binnig et al., 1986), by capacitance-detection (Neubauer et al., 1990; Göddenhenrich et al., 1990), and by four optical techniques namely (1) by optical interferometry (Mate et al., 1987 and Erlandsson et al., 1988) and with

optical fibers (Ruger et al., 1989 and Albrecht et al., 1992), (2) by optical polarization detection (Schonenberger and Alvarado, 1990), (3) by laser diode feedback (Sarid et al., 1988), and (4) by optical beam deflection (Meyer and Amer, 1988). The optical techniques are believed to be a more reliable and easily implemented detection method than tunneling (Bhushan, 1990; Sarid and Elings, 1991).

The first FFM was developed by Mate et al. (1987) at IBM Almaden Research Center. In their set up (Fig.2), the sample was mounted on three orthogonal piezoelectric tubes (PZT) (25 mm long), two of which (x, y axes) raster the sample in the surface plane with the third (z) moves the sample toward and away from the tip. A tungsten wire (12 mm long, 0.25 or 0.5 mm in diameter) was used as the cantilever. One end (the free end) of which was bent at a right angle and was electrochemically etched in NaOH solution to obtain a sharp point (150 to 300 nm in radius) to serve as the tip. The spring constants were 150 and 2500 N/m for the 0.25- and 0.5-mm diameter wires, respectively. Two laser beams were used independently to monitor cantilever deflection in the normal and parallel directions. A light beam was focused on the backside or edge of the lever by a microscope objective for normal and shear deflections, respectively. The interference pattern between the reflected and the reference beams reflected from the tungsten wire and an optical flat was projected on a photodiode to measure the instantaneous deflection of the lever as well as its vibration amplitude at high frequencies (Erlandsson et al., 1988). [More recently, a high-sensitivity fiber-optic displacement sensor has been developed by the IBM group which does not require specular reflection and is compact (Ruger et al., 1989; Albrecht et al., 1992).] The force in each direction was determined by multiplying the cantilever deflection by the spring stiffness of the cantilever in each direction. Mate et al. (1987) measured the friction of tungsten tip sliding against a freshly-cleaved HOP graphite by pushing the tip against the sample in the z-direction at desired loads (ranging from 7.5 to 56 μ N), and by moving the sample back and forth parallel to the surface plane at a velocity of 40 nm/s, and repeating the scanning by stepping the sample (for 3D profiling).

The second type of friction force microscopes were developed by Kaneko and his coworkers (Kaneko, 1988; Kaneko et al., 1991; Kaneko et al., 1992). One of their design is shown in Fig. 3. A diamond tip (0.1 mm radius) was held by a parallel-leaf spring unit (length: 10 mm, width: 1 mm, thickness: 20 μ m, spring constant: 3N/m). The sample was mounted on another parallel-leaf spring unit (length: 10 mm, width: 3 mm, thickness: 20-30 μ m, spring constant: 9-30 N/m). These parallel-leaf springs have greater torsional rigidity than single-leaf springs with the same spring constants. Thus deflection errors caused by tip movement are reduced by using parallel-leaf springs. A PZT tripod (16 μ m stroke at 100 V) was used for loading the sample against the tip as well as moving it in the two directions in the sample plane. A focusing error detection type optical head (resolution < 1 nm) was used to measure the tip displacement in the lateral (x) direction. A U-shape electromagnet was set to pull the tip assembly to overcome the frictional force. (An amorphous iron alloy plate was attached to the spring to obtain an effective pulling force.) Thus the friction force was measured by measuring the current that was required to hold the tip stationary. This design was modified later by Kaneko et al. (1991). The major modifications in the design are that (1) the sample is no longer supported by a parallel-leaf spring unit and is directly mounted to a PZT tube scanner (which may give more stability while scanning the sample), (2) the friction force (tip motion) is sensed by the voltage difference applied between two parallel electrodes rather than the current passing a coil around a magnet.

Figure 4 shows the new FFM design presented by Kaneko et al. (1991). A PZT tube scanner capable of 3D movement was used for moving and loading the sample against the tip. This scanner had an outer diameter of 10 mm, an inner diameter of 8 mm, and an effective length of 40 mm. For friction measurements, a diamond tip was used which was ground to the shape of a three-sided pyramid, whose point was sharpened to a radius of 0.1 μ m with an apex of 90 $^{\circ}$. The tip is mounted on one end of a single-leaf spring (length: 3-6.5 mm, width: 0.2 mm, thickness: 20 μ m, and spring constant: 0.3-3 N/m). The single-leaf spring was mounted perpendicular to a parallel-leaf spring unit (length: 5-10 mm, width: 1mm, thickness: 20 μ m, and spring constant: 3-24 N/m). The tip-to-sample contact was established by observing the parallel-leaf spring

vibration resulting from the vibrating tip; when in contact, there is an absence of parallel-leaf spring vibration. Applied normal force was obtained by the tube scanner displacement and the stiffness of the single-leaf spring. The tip assembly shown in Fig. 4 consists of two flat electrodes (2-mm square) attached to the ends of the parallel-leaf spring unit and an elastic member. The gap between the electrodes (typically 0.1 mm) is adjusted by a screw. The attractive force between the electrodes is controlled by the control unit to move the parallel-leaf spring to the zero-friction position. For friction measurement, the sample is scanned against the tip. The friction force being applied at the tip deflects the parallel-leaf spring which is sensed by an optical head. Control unit generates a voltage signal applied to the electrodes in order to move the associated leaf-spring back to zero displacement by overcoming the friction force. Thus, friction force is measured by measuring the required voltage difference between the electrodes.

Each of these instruments has its advantages and disadvantages. For example, the use of two laser beams in Mate et al.'s design adds an additional complexity in the design of the apparatus. Kaneko et al.'s design does not have the capability of measuring the surface topography and friction force simultaneously. The topography and friction force of their samples were measured separately (Kaneko et al., 1991). This is a significant drawback as any correlation between local variations in friction force and the surface topography can not be easily observed. However, friction force can be measured and calibrated relatively easily for both of these instruments.

In this study, we have chosen a modified friction force microscope from Digital Instruments (NanoScope III). This instrument is relatively simple to set and use and can provide simultaneous measurements of friction force and surface topography. The schematic of this instrument is shown in Fig. 5 and will be described in detail in the following section. The original design of this AFM version comes from Meyer and Amer (1988). The hardware modification of this instrument in order to measure friction force is also based on the same authors' suggestion (Meyer and Amer, 1990b). In terms of friction force measurement, there are several key issues relating to the use of this instrument have not been resolved. These include the basic operation of

the instrument to measure friction and the calibration of friction force. We will present a new method to measure friction and a calibration procedure to convert measured deflection data to forces.

3. Descriptions of a Commercial AFM and a New Friction Measurement Technique

3.1. The Apparatus

The basic design of a commercial AFM/FFM used in this study is shown in Fig. 5. The sample is mounted on a PZT tube scanner which consists of separate electrodes to precisely scan the sample in the x-y plane and to move the sample in the vertical (z) direction. A sharp tip at the free end of a microfabricated flexible cantilever is brought in contact with the sample. Features on the sample surface causes the cantilever to deflect in the vertical direction as the sample moves under the tip. A laser beam generated from a diode laser (light emitting diodes or LEDs) is directed by a prism onto the back of the cantilever near its free end, tilted downward at about 10^0 with respect to a horizontal plane. Reflected beam from the cantilever is directed through a mirror onto a split photodiode detector with four quadrants. The differential signal from the vertical two quadrants (top and bottom) of the photodiode detector $[(T-B)/(T+B)]$ provides a sensitive measure of the cantilever vertical deflection. We call this signal "AFM" signal. This AFM signal is used as the feedback signal to control the vertical location of the PZT tube scanner and the sample, such that the cantilever vertical deflection (hence the normal force at the tip-sample interface) will remain (almost) constant as the sample is scanned. Thus the vertical motion of the tube scanner relates directly to the topography of the sample surface. This mode of operation is referred as "height" mode. (We note that normal force and vertical motion of the sample can be independently measured by photodiode and PZT scanner, respectively.) Friction force can also be measured in the height mode (referred to as method 1 in Fig. 6). The other two quadrants of the photodiode detector ("L" and "R") are arranged horizontally. Their purpose is to measure the "lateral", or "frictional" force exerted to the cantilever by the sample in the so called "aux" mode (referred to as method 2 in Fig. 6). If the sample is scanned back and forth in x

direction as shown in Fig. 6, friction force between the sample and the tip will produce a twisting of the cantilever in the x direction, schematically shown in Fig. 6b (right). The laser beam will be reflected out of the plane defined by the incident beam and the vertically reflected beam from an untwisted cantilever. This produces an intensity difference of the laser beam received between the left and right ("L" and "R") quadrants of the detector. The degree of twisting, hence the intensity difference between the left and right quadrants of the detector $[(L-R)/(L+R)]$, is directly related to the magnitude of friction force. The differential signal between the left and the right detectors is called "FFM" signal.

Silicon nitride cantilevers with integrated square pyramidal tips produced by plasma-enhanced chemical-vapor-deposition (PECVD) (Albrecht et al., 1990) are generally used in this AFM/FFM, Fig. 5b. The length of the cantilever beams (from the substrate to the apex of the triangular cantilever) is either 115 or 193 μm , base width of 122 or 205 μm , and thickness is 0.55 μm with spring constants ranging from 0.06 to 0.58 N/m and natural frequency ranging from 8 to 40 kHz. The pyramidal tips are highly symmetric with its end having a radius of about 20-50 nm. The tip side walls have a slope of 35° and the length of the edges of the tip at the cantilever base is about 4 μm . We have also coated some of the tips with either Ni (~ 11 nm) by thermal evaporation to investigate their friction behavior. Conical diamond tips sharpened to a radius of about 100 nm with a 60° apex angle and attached to a single-leaf spring (20 μm in thickness and 0.2 mm in width) have also been used in this AFM/FFM (Kaneko and Oguchi, 1990).

The maximum scan length of this instrument ranges from about 0.7 μm to about 125 μm with different scanners. PZT materials are nonlinear and large scans may give distorted data, therefore these are scan length limited. For large samples (larger than about 25 mm x 25 mm) which can not be fitted into the AFM assembly, stand alone AFMs can be used. In these units, the sample is stationary. The cantilever beam and the compact assembly of laser source and detector are attached to the free end of a PZT transducer which drives the tip over the stationary sample.

Since the cantilever beam and detector assembly are scanned instead of the sample, some vibration are possible and lateral resolution of these instruments is reduced. In the stand alone AFMs, a single photodetector, instead of split photodiode detector is used. As a result , friction force measurement can not be made.

3.2 Friction Measurement Methods

We define a scanning angle to be the angle relative to the y-axis in Fig. 6a. This is also the long axis of the cantilever. A zero degree scanning angle corresponds to the sample scanning in the y direction, and a 90 degree scanning angle corresponds to the sample scanning perpendicular to this axis in the xy plane (in x axis). If the scanning angle is in both y and -y directions, we call this "parallel scan". Similarly, a "perpendicular scan" means the scanning direction is in x and -x directions. Two methods of measuring friction force will be discussed in this paper. The sample traveling direction for each of these two methods is illustrated in Fig. 6b.

We note that *topographic* measurements are made using "height" mode (defined early) at any scanning angle. At a first instance, scanning angle may not appear to be an important parameter. However, the friction force between the tip and the sample (which we will discuss later) will affect the topographic measurements in a parallel scan. Therefore a perpendicular scan may be more desirable. Generally, one picks a scanning angle which gives the same topographic data in both directions; this angle may be slightly different than that for the perpendicular scan.

3.2.1 Method 1 -- "Height" mode with parallel scans.

In addition to conduct topographic imaging, it is also possible to measure friction force using "height" mode when the scanning direction of the sample is parallel to *y direction* (parallel scan). If there were no friction force between the tip and the moving sample, the topographic feature would be the only factor which cause the cantilever to be deflected vertically. However, friction force does exist on all contact surfaces where one object is moving relative to another. The friction force between the sample and the tip will also cause a cantilever deflection. We assume

that the normal force between the sample and the tip is W_0 when the sample is stationary (W_0 is typically in the range of 10 nN to 200 nN), and the friction force between the sample and the tip is W_f as the sample scans against the tip. The direction of friction force (W_f) is reversed as the scanning direction of the sample is reversed from positive (y) to negative (-y) directions ($\bar{W}_{f(y)} = -\bar{W}_{f(-y)}$).

When the vertical cantilever deflection is set at a constant level, it is the total force (normal force and friction force) applied to the cantilever that keeps the cantilever deflection at this level. Since the friction force is in opposite directions as the traveling direction of the sample is reversed, the normal force will have to be adjusted accordingly when the sample reverses its traveling direction, so that the total deflection of the cantilever will remain to be the same. We can calculate the difference of the normal force between the two traveling directions for a given friction force W_f . First, by means of a constant deflection, the total moment applied to the cantilever is constant. If we take the reference point to be the point where the cantilever joins the cantilever holder (substrate), point P in Fig. 7, we have the following relationship:

$$(W_0 - \Delta W_1) L + W_f l = (W_0 + \Delta W_2) L - W_f l, \quad (1)$$

or

$$(\Delta W_1 + \Delta W_2) L = 2 W_f l. \quad (2)$$

Thus

$$W_f = (\Delta W_1 + \Delta W_2) L / (2 l), \quad (3)$$

where ΔW_1 and ΔW_2 are the absolute value of the changes of normal force when the sample is traveling in -y and y directions, respectively, as shown in Fig 7; L is the length of the cantilever; l is vertical distance between the end of the tip and point P. The coefficient of friction (μ) between the tip and the sample is then given as

$$\mu = W_f / W_0 = (\Delta W_1 + \Delta W_2) / W_0 (L/2 l). \quad (4)$$

In all circumstances, there is an adhesive force (attractive force) between the cantilever tip and the sample because of water from the air and other contaminants present at the surface which form meniscus bridges (Blackman et al. 1990, O'Shea and Welland, 1992). If this adhesive force (and indentation effect as well, which is usually small for rigid samples) can be neglected, the normal force W_0 is then equal to the initial cantilever deflection H_0 multiplied by the spring constant of the cantilever. $(\Delta H_1 + \Delta H_2)$ can be measured by multiplying the same spring constant by the height difference of the PZT between the two traveling directions (y and -y directions) of the sample. This height difference is denoted as $(\Delta H_1 + \Delta H_2)$, shown schematically in Fig. 8. Thus, Eq. 4 can be rewritten as

$$\mu = W_f / W_0 = (\Delta H_1 + \Delta H_2) / H_0(L/2l). \quad (5)$$

Since the PZT vertical position is affected by the surface topographic profile of the sample in addition to the friction force being applied at the tip, this difference has to be taken point by point at the same location on the sample surface as shown in Fig. 8. Subtraction of point by point measurements may introduce errors. We will come back to this point later. In addition, precise measurement of L and l (which should include the cantilever angle) are also required.

If the adhesive force between the tip and the sample is large enough that it can not be neglected, one should include it in the calculation. However, there could be a large uncertainty in determining this force, thus an uncertainty in using Eq. 5. An alternative approach is to make the measurements at different normal loads and to use $\Delta(H_0)$ and $\Delta(\Delta H_1 + \Delta H_2)$ from the measurements in Eq. 5. Another comment on Eq. 5 is that, since it is only the ratio between $(\Delta H_1 + \Delta H_2)$ and H_0 comes into this equation, the PZT vertical position H_0 and its position difference $(\Delta H_1 + \Delta H_2)$ can be in the units of volts (as long as the vertical traveling distance of the PZT and the voltage applied to it has a linear relationship).

It should also be pointed out that, Eqs. 4 and 5 are derived under the assumption that the friction force W_f is the same for the two scanning directions of the sample. This is an

approximation since the normal force is slightly different for the two scans as well as there may be directionality effect in friction. However, this difference is much smaller compared to W_0 itself. We can ignore the second order correction.

3.2.2 Method 2 -- "Aux" mode with perpendicular scan and suggested modifications

Another method to measure friction is the one suggested by Meyer and Amer (1990b). The sample is scanned perpendicular to the long axis of the cantilever beam (i.e., to scan along the x or -x direction in Fig. 6a) and the output of the horizontal two quadrants of the photodiode-detector is measured. In this arrangement, as the sample moves under the tip, the friction force will cause the cantilever to twist. Therefore the light intensity between the left and right (L and R in Fig. 6b, right) detectors will be different. The differential signal between the left and right detectors is denoted as FFM signal $[(L-R)/(L+R)]$. This signal can be related to the degree of twisting, hence to the magnitude of friction force. Again, because of a possible error in determining normal force due to the presence of an adhesive force at the tip-sample interface, the slope of the friction data (FFM signal vs. normal load) needs to be taken for an accurate value of coefficient of friction.

While friction force contributes to the FFM signal, friction force may not be the only contributing factor in the present set up of commercial FFM instruments (for example, NanoScope III). One can notice this fact by simply engaging the cantilever tip with the sample. Before engaging, the left and right detectors can be balanced by adjusting the position of the detectors so that the intensity difference between these two detectors is zero (FFM signal is zero). Once the tip is engaged with the sample, this signal is no longer zero even if the sample is not moving in the xy plane with no friction force applied. This would be a detrimental effect. It has to be understood and eliminated from the data acquisition before any quantitative measurement of friction force becomes possible.

One of the fundamental reasons for this observation is the following. The detectors may not have been properly aligned with respect to the laser beam. To be precise, the vertical axis of the detector assembly (the line joining T-B in Fig. 9) is not in the plane defined by the incident laser beam and the beam reflected from an untwisted cantilever (we call this plane "beam plane"). When the cantilever vertical deflection changes due to a change of applied normal force (without having the sample scanned in the xy plane), the laser beam will be reflected up and down and form a projected trajectory on the detector. (Note that this trajectory is in the defined beam plane). If this trajectory is not coincident with the vertical axis of the detector, the laser beam will not evenly bisect the left and right quadrants of the detectors, even under the condition of no torsional motion of the cantilever, see Fig 9. Thus when the laser is reflected up and down due a change of the normal force, the intensity difference between the left and right detectors will also change. In other words, the FFM signal will change as the normal force applied to the tip is changed, even if the tip is not experiencing any friction force. This (FFM) signal is unrelated to friction force or to the actual twisting of the cantilever. We will call this part of FFM signal " FFM_F ", and the part which is truly related to friction force " FFM_T ".

The FFM_F signal can be eliminated. One way of doing this is as follows. First the sample is scanned in both x and $-x$ directions and the FFM signal for scans in each direction is recorded. Since friction force reverses its directions when the scanning direction is reversed from x to $-x$ direction, the FFM_T signal will have opposite signs as the scanning direction of the sample is reversed ($FFM_T(x) = -FFM_T(-x)$). Hence the FFM_T signal will be canceled out if we take the sum of the FFM signals for the two scans. The average value of the two scans will be related to FFM_F due to the misalignment,

$$FFM(x) + FFM(-x) = 2FFM_F. \quad (6)$$

This value can therefore be subtracted from the original FFM signals of each of these two scans to obtain the true FFM signal (FFM_T). Or, alternately, by taking the difference of the two FFM signals, one directly gets the FFM_T value

$$\begin{aligned}
 FFM(x) - FFM(-x) &= FFM_T(x) - FFM_T(-x) \\
 &= 2FFM_T(x).
 \end{aligned} \tag{7}$$

To show the significance that it is necessary to scan the sample in both x and $-x$ directions, and to take the differential FFM signal as the friction signal, we show in Fig. 10 a single direction measurement result for graphite. The horizontal axis in this figure is the cantilever deflection and the vertical axis is the average of FFM or FFM_T signal over a $1 \mu\text{m} \times 1 \mu\text{m}$ scan area. During the measurement, the sample is moved in x and $-x$ direction at a velocity of $4 \mu\text{m/s}$, and slowly stepped in y direction (16 nm/s) with a 4 nm step size to scan the whole area. The open and filled circles in the figure correspond to FFM signals in x and $-x$ directions respectively. We see that the slopes of these two curves are almost the same and is comparable to the data taken for several other samples. It is only the difference between these two curves, or the FFM_T signal (represented by the third curve with open triangles), that gives a meaningful and reproducible data.

3.2.3 A Comparison Between These Two Methods

The method of using "height" mode and parallel scan (method 1) is very simple to use. Technically, this method can provide 3D friction profiles and the corresponding topographic profiles. However, there are some problems with this method. Under most circumstances, the PZT scanner displays a hysteresis when the traveling direction of the sample is reversed. Therefore the measured surface topographic profiles will be shifted relative to each other along the y -axis for the two opposite (y and $-y$) scans. This would make it difficult to measure the local height difference of the PZT for the two scans. However, the average height difference between the two scans and hence the average friction can still be measured. The measurement of average friction can serve as an internal means of friction force calibration.

Method 2 is a more desirable approach. The subtraction of FFM_T signal from FFM for the two scans does not introduce error to local friction force data. An ideal approach in using this

method would be to add the average value of the two profiles in order to get the error component (FFM_F) and then subtract this component from either profiles to get true friction profiles in either directions. By making measurements at various load, we can get average value of the coefficient of friction which then can be used to convert the friction profile to the coefficient of friction profile. Thus any directionality and local variations in friction can be easily measured. In this method, since topography data are not affected by friction, accurate topography data can be measured simultaneously with friction data and better localized relationship between the two can be established.

3.2.4 Normal Force and Friction Force Calibrations

In order to calculate the absolute value of normal and friction forces in Newtons using the measured AFM and FFM_T voltage signals, it is necessary to first have an accurate value of the spring constant of the cantilever (k_c). The spring constant can be calculated using the geometry and the physical properties of the cantilever material. However, the properties of the PECVD Si_3N_4 (used in fabricating cantilevers) could be different from that of bulk material. For example, by using an ultrasonic measurement, we found the Young's modulus of the cantilever beam to be about 238 ± 18 GPa which is less than that of bulk Si_3N_4 (310 GPa). Furthermore the thickness of the beam is nonuniform and difficult to measure precisely. Since the stiffness of a beam goes as the cubic of thickness, minor errors in precise measurements of thickness can introduce substantial stiffness errors. Thus one should experimentally measure the spring constant of the cantilever. For normal stiffness measurement, we used a stainless steel spring sheet of known stiffness (width: 1.35 mm, thickness: 15 μm , free hanging length: 5.2 mm). One end of the spring was attached to the sample holder and the other end was free for movement and was made to contact with the cantilever tip, see Fig. 11. We measured the PZT traveling distance for a given cantilever deflection. For a rigidly mounted sample, the PZT traveling distance Z , (measured from the point where the tip touches the sample) should equal the cantilever deflection. To keep the cantilever deflection at the same level using a flexible spring sheet, the

new PZT traveling distance Z_t' , would be different from Z_t . The difference between Z_t' and Z_t corresponds to the deflection of the spring sheet. If the spring constant of the spring sheet is k_s , the spring constant of the cantilever k_c can be calculated by

$$(Z_t' - Z_t)k_s = Z_t k_c,$$

or $k_c = k_s(Z_t' - Z_t)/Z_t$. (8)

The spring constant of the spring sheet (k_s) used in this study is calculated to be 1.54 N/m. For a typical cantilever used in our study (length: 115 μm , base width: 122 μm , and thickness: 0.6 μm), k_c was measured to be 0.40 N/m. To relate photodiode detector output to the cantilever deflection in nm, we use the same rigid sample to push against the AFM tip. Since for a rigid sample the cantilever vertical deflection equals the sample traveling distance measured from the point where the tip touches the sample, the photodiode output as the tip is pushed by the sample can be converted directly to cantilever deflection. For our measurements, we found the conversion to be 20 nm/V.

The normal force applied to the tip can be calculated by multiplying the cantilever vertical deflection by the lever spring constant for samples which have very small adhesive force with the tip. If the adhesive force between the sample and the tip is large, it should be included in the normal force calculation. This is particularly important in atomic- scale force measurement because in this region, the typical normal force that we measure is in the range of a few hundreds of nN to a few μN . The adhesive force could be comparable to the applied force. The magnitude of the adhesive force is determined by multiplying the maximum cantilever deflection in the downward direction before the tip is pulled off the sample surface, by the spring constant of the cantilever. Figure 12 shows an example of cantilever deflection as a function of sample position (height). "Extending" means the sample is pushed towards the tip and "retracting" means the sample is pulled away from the tip. As the sample surface approaches the tip within a few nm (point A), an attractive force exists between the atoms of the tip surface and the atoms of the sample surface. The tip is pulled toward the sample and the contact occurs at point B. As the

sample is pushed further against the tip, the force at the interface increases and the cantilever is deflected upward. This deflection equals the sample traveling distance measured from point B for a rigid sample. As the sample is retracted, the force is reduced. At point C in the retracting curve, the sample is disengaged from the tip. Before the disengagement, the tip is pulled toward downward direction due to the attractive force. The force that is required to pull the tip away from the sample is the force that equals (but in the opposite direction with) the adhesive force. This force is calculated by the maximum cantilever deflection in the downward direction times the spring constant of the cantilever. The maximum cantilever deflection in downward direction is just the horizontal distance between points B and C in this curve. We measured this distance to be about 200 nm in this curve which corresponds to an adhesive force of 80 nN for a spring constant of 0.4 N/m. Friction force at a zero cantilever deflection is associated with this force between the sample and the tip. Since the calculation of both the externally applied and adhesive forces involves the same spring constant of the cantilever, the total normal force (once the sample and the tip are in contact) is equal to the spring constant times the cantilever "deflection" measured right before the pull off point in the retracting curve. This "deflection" is also the PZT traveling distance measured from point C toward the tip for a rigid sample. Although the calculation of adhesive force is important in the calculation of normal force, it is not important in the calculation of coefficient of friction if we take the slope of friction force vs. normal force curve.

The conversion of friction signal (from FFM_T to friction force) is not as straightforward. For example, one can calculate the degree of twisting for a given friction force using the geometry and the physical properties of the cantilever (Meyer and Amer, 1988; O'Shea and Welland, 1992). One would need the information on the detectors such as the quantum efficiency of the detector, the laser power, the instrument's gain, etc. in order to be able convert the signal into the degree of twisting. Generally speaking, this procedure can not be accomplished without having some detailed information about the instrument. And this information is not usually provided by the manufacturer. Even if this information is readily available, error may still occur

in using this approach because there will always be variations as a result of the instrumental set up. For example, it has been noticed that the measured FFM_T signal could be different for the same sample when different AFM microscopes of the same kind are used. The essence is that, one can not calibrate the instrument experimentally using this calculation. O'Shea and Welland (1992) did perform a calibration procedure in which the torsional signal was measured as the sample is displaced a known distance laterally while ensuring that the tip does not slide over the surface. However, it is difficult to verify if the tip sliding does not occur.

Apparently, a new method of calibration is required. There is a more direct and simpler way of doing this. The first method described (method 1) to measure friction can directly provide an absolute value of coefficient of friction. It can therefore be used just as an internal means of calibration for the data obtained using method 2. Or for a polished sample which introduces least error in friction measurement using method 1, method 1 can be used to obtain calibration for friction force for method 2. Then this calibration can be used for measurement on all samples using method 2. In method 1, the length of the cantilever required can be measured using an optical microscope; the length of the tip can be measured using a scanning electron microscope. The relative angle between the cantilever and the horizontal sample surface can be measured directly. Thus the coefficient of friction can be measured with little unknown parameters. The friction force can then be calculated by multiplying the coefficient of friction by the normal load. The FFM_T signal obtained using method 2 can then be converted into friction force. For our instrument, we found the conversion to be 8.6 nN/V.

4 Results and discussion

Friction of Pt (rms roughness 0.22 nm, calibration grid with $10 \mu m \times 10 \mu m$ grid dimension from Digital Instruments) and polished natural diamond and silicon (rms roughness of 2.3 nm and 0.14 nm respectively over an one μm area) were measured against a Si_3N_4 tip using both methods 1 and 2. The result on Pt (measured using both methods 1 and 2) is used to calibrate the friction data of other samples obtained using method 2. And these data were compared with those

obtained using method 1 for each sample to examine the consistency between these two methods. Some of the tips were coated with 11 nm of Ni and were also used for the measurements.

We first show in Fig.13 an example of a typical trajectory of the PZT vertical height as the AFM tip is scanned in both y and -y directions across a Pt surface. For a smooth sample like this, the separation between these two trajectories can easily be measured. We have measured the height difference of the PZT ($\Delta H_1 + \Delta H_2$) at different normal loads (H_0), and used $\Delta(\Delta H_1 + \Delta H_2)$ and $\Delta(H_0)$ in equation (5) to calculate μ . Figure 14 shows the data from three sets of measurements at various loads on Pt. The horizontal axis is the center position of the PZT scanner and the vertical axis is the average (over an 1 μm scan length) height difference of the PZT between y and -y scans. During the measurement, the PZT center position is changed by setting the $[(T-B)/(T+B)]$ signal at different values for the feedback circuit. The resulting height difference of the PZT between the two scans (y and -y) was measured and averaged over the scan length. We see in Fig. 14 that all data fall closely on a straight line. The slope (best linear fit) of this curve is 9.4×10^{-3} . Using the geometry of the cantilever and the tip ($L=115 \mu\text{m}$ $l=10 \mu\text{m}$ in Eq. (4)), value of coefficient of friction of 0.054 is obtained.

Figure 15 is obtained for Pt using method 2. Here, the cantilever vertical deflection vs. the friction signal (half of the difference of the FFM signals between the x and -x scans, or $\text{FFM}_T(x)$ signal) is plotted. The data were obtained in the same way as for Fig. 10: the sample was moved in x and -x direction at a velocity of 4 $\mu\text{m/s}$, and slowly stepped (by 4 nm/step) in y direction (16 nm/s) to scan the whole area (1 $\mu\text{m} \times 1 \mu\text{m}$). The data (averaged over the scan area) for each measurement can be fitted into a straight line. To show the statistical variation between different measurements, eleven sets of measurements at various loads were made and were plotted in this figure. Again, a good linear fit of the data has been observed with a slope of 2.5 mV/nm. Using the value of coefficient of friction calculated previously, we calculate that a slope of 1 mV/nm in this curve corresponds to a coefficient of friction 0.022. Using the spring constant of the

cantilever (0.4 N/m), we then calculated that a 1 V in this curve (FFM_T signal) corresponds to a friction force of 8.7 nN.

Similar measurements were made on diamond and silicon. We use the values obtained above for Pt, and the slopes of the curves of these two samples (diamond and silicon) obtained using method 2 to calculate their coefficient of friction. The data were compared with those obtained directly using method 1 for the corresponding samples. For simplicity, we summarize the result in Table 1. A reasonable agreement between the measurements using the two methods is obtained. Friction data for aluminum and graphite are also included in Table 1. Method 1 was not used for these samples since a good agreement is obtained between methods 1 and 2. In addition, our aluminum sample is not polished and has a very rough surface. Method 1 is difficult to apply to this sample. The friction force for all tips against graphite is so small that it can not be directly measured using method 1. Even with method 2, we find that the signal variation at different applied normal forces is also within the range of experimental uncertainty. The slope that best fit to the data with uncoated tip is 3×10^{-4} (V/nm), which corresponds to a coefficient of friction 0.006. This value is listed in Table 1. [The coefficient of friction of graphite against a tungsten tip was reported to be 0.012 according to Mate et al. (1987)]. A friction force vs. normal force plot for diamond, HF cleaned silicon, and graphite are shown in Fig. 16. The result of metal coated tips is not significantly different from that of uncoated tips, Table 1.

We also made macrofriction measurements using a 5 mm diameter silicon nitride ball sliding against various samples under the following condition: reciprocating amplitude -0.8 mm, frequency -1Hz, and normal load=1N. The data are also reported in Table 1. We note that the atomic scale coefficient of friction is small compared to that of macroscopic coefficient of friction. There may be fundamental reasons for this observation. For example, in macroscopic measurements, the interlocking of asperities between the sample and the mating surface (plowing components) may play a significant role to the macroscopic friction. In atomic scale measurement under extremely low loads (< 400 nN), plowing contribution may be less significant. Hirano

and Shinjo (1990) have reported that under some conditions, atomic-scale friction may vanish completely.

Finally, we have shown that a misalignment between the laser beam and the detector assembly could produce an FFM signal which is unrelated to friction. This effect can be eliminated with some AFM hardware improvements. Fig. 17 shows one of the sources which cause the misalignment. The cantilever substrate has two cantilevers at each end, one is about 100 μm in length (C1) and the other is about 200 μm (C2). The laser beam is brought onto one of the two cantilevers by adjusting the angle of a platform (a prism, a laser diode, and a lens are mounted in the platform). By doing this, the beam is not really vertically incident on the cantilever. Hence the trajectory of the reflected beam will almost always be at an angle relative to the detector vertical axis as shown in the insets. For this reason, the FFM signal will change (possibly linearly) as the cantilever is vertically deflected. But this is not associated with friction force. If, instead of tilting the incident laser beam by tilting the platform as shown in Fig. 17, the cantilever holder is translated by a translating fixture, it is possible to have any one of these cantilevers intercepting the laser beam while keeping the beam vertical and unchanged. In this way, it is possible to have the photodetector vertical axis aligned in the laser beam plane, and the apparent artifact will no longer exist.

5. Summary

Existing FFMs and their operating principles have been reviewed. Two new measurement methods are introduced. Method 1 is to scan the sample along the long axis of the cantilever with the AFM operated in "height" mode. While with method 2, samples are scanned in the direction perpendicular to the long axis of the cantilever with the FFM operated in "aux" mode. These two methods are complimentary to each other. Method 1 can be used as an internal means of instrumental calibration for method 2. Method 2 can be used easily to measure local friction force profiles in either scan directions as well as surface topographic profiles simultaneously. The proposed modification to eliminate the instrumental misalignment problem is able to produce

reproducible measurements. The calibration of normal force, including the measurement of cantilever spring constant and taking into account of adhesive force between the sample and the cantilever tip, has been discussed. Procedures of converting the FFM signal into friction forces is described. Possible instrumental improvements towards easier operation (without the need of taking the differential FFM signals) are suggested. The coefficient of friction of several materials against Ni coated and uncoated Si_3N_4 tip have been measured. We find that the atomic-scale coefficient of friction for all the sample-tip combinations is small as compared to macroscopic measurements with silicon nitride balls.

Acknowledgments

We thank Dr. V. Elings of Digital Instruments Inc. for many discussions, Dr. R. Kaneko of NTT Japan for suggesting a method to measure the cantilever spring constant and Dr. B. K. Gupta for macrofriction measurements. This paper in part is based on a technical surveillance report presented to ASME Research Committee on Tribology by the second author. This research was sponsored in part by the Department of the Navy, Office of the Chief of Naval Research. The contents of the information does not necessarily reflect the position or the policy of the Government, and no official endorsement should be inferred.

References

Albrecht, T. R., Akamine, S., Carver, T. E., and Quate, C. F., (1990) "Microfabrication of Cantilever Styli for the Atomic Force Microscope", J. Vac. Sci and Technol. A, Vol. 8, No. 4, pp. 3386-3396.

Albrecht, T. R., Grutter, P., Ruger, D. and Smith, D. P. E. (1992), "Low Temperature Force Microscope with All-Fiber Interferometer", Ultramicroscopy, Vol. 42-44, pp. 1638-1646.

Albrecht, T. R. and Quate, C. F. (1987), "Atomic Resolution Imaging of a Nonconductor by Atomic Force Microscopy", J. Appl. Phys., Vol. 62, No. 7, pp. 2599-2602.

Bhushan, B. (1990), Tribology and Mechanics of Magnetic Storage Devices, Springer Verleg, New York.

Bhushan, B. (1993), "Tribology of Magnetic Head-Medium-Interface", in NATO-ASI Volume on High Density Digital Recording, Kluwer Academic Publisher, Dordrecht, Netherlands.

Bhushan, B. and Blackman, G. S. (1991), "Atomic Force Microscopy of Magnetic Rigid Disks and Sliders and Its Applications to Tribology", J. Trib., Trans. ASME, Vol. 113, pp. 452-458.

Binnig, G., Rohrer, H., Gerber, Ch. and Weibel, E. (1982), "Surface Studies by Scanning Tunneling Microscopy", Phys. Rev. Lett., Vol. 49, No. 1, pp. 57-61.

Binnig, G., Quate, C. F. and Gerber, Ch. (1986), "Atomic Force Microscope", Phys. Rev. Lett., Vol. 56, No. 9, pp. 930-933.

Blackman, G. S., Mate, C. M. and Philpott, M. R. (1990), "Interaction Forces of a Sharp Tungsten Tip with Molecular Films on Silicon Surfaces", Phys. Rev. Lett., Vol. 65, No. 18, pp. 2270-2273.

Erlandsson, R., McClelland, G. M., Mate, C. M. and Chiang, S. (1988), "Atomic Force Microscopy Using Optical Interferometry", J. Vac. Sci. Technol. A, Vol. 6, No. 2, pp. 266-270.

Göddenhenrich, T., Lemke, H., Hartmann, U. and Heiden, C. (1990), "Force Microscope with Capacitive Displacement Detection", J. Vac. Sci. Technol. A, Vol. 8, No. 1, pp. 383-387.

Grütter, P., Ruger, D., Mamin, H. J., Castillo, G., Lin, C.-J., McFadyen, I. R., Valletta, R. M., Wolter, O., Bayer, T., and Greschner, J. (1991), "Magnetic Force Microscopy with Batch-Fabricated Force Sensors", J. Appl. Phys., Vol. 69, No. 8, pp. 5883-5885.

Hirano, M. and Shinjo, K. (1990), "Atomistic Locking and Friction", Phys. Rev. B, Vol. 41, No. 17, pp. 11837-11851.

Kaneko, R. (1988), "A Friction Force Microscope Controlled with an Electromagnet", J. Microscopy, Vol. 152, Pt.2, pp.363-369.

Kaneko, R. and Enomoto, Y. (eds.) (1992), Proc. 1st Int. Workshop on Microtribology, The Jap. Soc. of Tribologists, Tokyo, Japan, October.

Kaneko, R., Miyamoto, T. and Hamada, E. (1991), "Development of a Controlled Friction Force Microscope and Imaging of Recording Disk Surfaces", Adv. Info. Storage Syst., Vol. 1, pp. 267-277.

Kaneko, R., and Oguchi, S. (1990), "Ion-Implanted Diamond Tip for a Scanning Tunneling Microscope", Jap. J. Appl. Phys., Vol. 28, No. 9, pp. 1854-1855.

Kaneko, R., Oguchi, S., Hara, S., Matsuda, R., Okada, T., Ogawa, H. and Nakamura, Y. (1992), "Atomic Force Microscope Coupled with an Optical Microscope", Ultramicroscopy, Vol. 42-44, pp. 1542-1548.

Maivald, P., Butt, H. J., Gould, S. A. C., Prater, C. B., Drake, B., Gurley, J. A., Elings, V. B. and Hansma, P. K. (1991), "Using Force Modulation to Image Surface Elasticities with the Atomic Force Microscope", Nanotechnology, Vol. 2, No. 2, pp. 103-106.

Manne, S., Hansma, P. K., Massie, J., Elings, V. B. and Gewirth, A. A. (1991), "Atomic-Resolution Electrochemistry with the Atomic Force Microscope: Copper Deposition on Gold", Science, Vol. 251, pp. 183-186.

Marti, O., Drake, B. and Hansma, P. K., (1987) "Atomic Force Microscopy of Liquid-Covered Surfaces: Atomic Resolution Images", Appl. Phys. Lett., Vol. 51, No. 7, pp. 484-486.

Martin, Y., Wickramasinghe, H. K. (1987), "Magnetic Imaging by Force Microscopy with 1000 Å Resolution", Appl. Phys. Lett., Vol. 50, No. 20, pp. 1455-1457.

Mate, C. M., McClelland, G. M., Erlandsson, R., and Chiang, S. (1987), "Atomic-Scale Friction of a Tungsten Tip on a Graphite Surface", Phys. Rev. Lett., Vol. 59, No. 17, pp. 1942-1945.

Melmed, A. J. (1991), "The Art and Science and Other Aspects of Making Sharp Tips", J. Vac. Sci. Technol. B, Vol. 9, No. 2, pp. 601-608.

Meyer, G and Amer, N. M. (1988), "Novel Optical Approach to Atomic Force Microscopy", Appl. Phys. Lett., Vol. 53, No. 12, pp. 1045-1047.

Meyer, G. and Amer, N. M. (1990a), "Optical-Beam-Deflection Atomic Force Microscopy: The NaCl (001) Surface", Appl. Phys. Lett., Vol. 56, No. 21, pp. 2100-2101.

Meyer, G. and Amer, N. M. (1990b), "Simultaneous Measurement of Lateral and Normal Forces with an Optical-Beam-Deflection Atomic Force Microscope", Appl. Phys. Lett., Vol. 57, No. 20, pp. 2089-2091.

Neubauer, G., Cohen, S. R., McClelland, G. M., Horne, D. and Mate C. M. (1990), "Force Microscopy with a Bidirectional Capacitance Sensor", Rev. Sci. Instrum., Vol. 61, No. 9, pp. 2296-2308.

Ohkubo, T., Kishigami, J., Yanagisawa, K., and Kaneko, R. (1991), "Submicron Magnetizing and Its Detection Based on the Point Magnetic Recording Concept", IEEE Trans. Magn., Vol. 27, No. 6, pp. 5286-5288,

O'Shea, S. J. and Welland, M. E. (1992), "Atomic Force Microscope Study of Boundary Layer Lubrication", Appl. Phys. Lett., Vol. 61, No. 18, pp. 2240-2242.

Ruan, J. and Bhushan, B. (1993), "Atomic Force Microscope and Scanning Tunneling Microscope Studies of Fullerene Films", J. Mat. Res. (in press).

Ruger, D., Mamin, H. J. and Guethner, P. (1989), "Improved Fiber-Optical Interferometer for Atomic Force Microscopy", Appl. Phys. Lett., Vol. 55, No. 25, pp. 2588-2590.

Sarid, D. and Elings, V. (1991), "Review of Scanning Force Microscopy", J. Vac. Sci. Technol. B, Vol. 9, No. 2, pp. 431-437.

Sarid, D., Iams, D., Weissenberger, V. and Bell, L. S. (1988), "Compact Scanning-Force Microscope Using Laser Diode", Optics Letters, Vol. 13, No. 12, pp. 1057-1059.

Schonenberger, C. and Alvarado, S. F. (1990), "Understanding Magnetic Force Microscopy", Z. Phys. B, (Germany) Vol. 80, No. 3, pp. 373-83.

Table 1. Atomic-scale friction and macrofriction data of various samples

| Sample | Coefficient of friction | | | |
|------------------------------|---|---|-----------------------------|--------------------|
| | FFM measurements | | | Macro measurements |
| | Method 1 with Si_3N_4 tip | Method 2 with Si_3N_4 tip | Method 2 with Ni-coated tip | |
| Silicon (HF cleaned) | 0.07 | 0.08 | | |
| Silicon (before HF cleaning) | 0.06 | 0.06 | 0.07 | 0.4 |
| Natural diamond | 0.04 | 0.05 | 0.07 | 0.2 |
| Platinum | 0.054 | 0.054 | 0.06 | 0.3 |
| Aluminum | | 0.08 | 0.09 | 0.6 |
| Graphite | | ~0.006 | ~0.006 | 0.1 |

Figure captions

Fig. 1 Schematic of an AFM which uses optical interference to detect the lever deflection (Erlandsson et al., 1988).

Fig. 2 Schematic of the FFM by Mate et al. (1987). Normal and friction forces are measured by measuring the cantilever deflection in both normal and lateral directions by optical interference.

Fig. 3 Schematic of FFM by Kaneko (1988). (a) The over all set up showing the tip assembly (sample support assembly not shown) and the associated instrumentation, (b) parallel spring unit for supporting and loading the sample. Normal force is measured by the deflection of the parallel spring unit in (b). Friction force is measured by measuring the current that is required to hold the tip stationary; the tip displacement is sensed by the optical head.

Fig. 4 Schematic of FFM by Kaneko et al. (1991). Sample is mounted directly on the PZT as opposed on a parallel spring unit in Fig. 3.

Fig. 5 (a) Schematic of FFM used in this study. The vertical deflection (normal force) of the cantilever is measured by the top (T) and bottom (B) quadrants of the photodetector. The surface topography is measured by measuring the z-travel of PZT scanner that is required to keep the cantilever vertical deflection $[(T-B)/(T+B)]$ constant. Lateral deflection (friction force) is measured by the left (L) and right (R) quadrants of the photodetector. Friction force is a function of $[(L-R)/(L+R)]$, (b) Schematic of the PECVD Si_3N_4 cantilever beam with tip used.

Fig. 6 (a) Schematics defining the x and y directions relative to the cantilever, and showing the sample traveling direction in two different measurement methods discussed in the text, (b) deformation of the tip/cantilever shown as a result of sliding in the x and y directions. A twist is introduced to the cantilever if the scanning is in x direction [(b), right].

Fig. 7 Schematic showing an additional bending of the cantilever due to friction force when the sample is scanned in y or -y directions (left). This effect will be canceled by adjusting the PZT height by a feedback circuit (right).

Fig. 8 Schematic illustration of the height difference of the PZT tube scanner as the sample is scanned in y and -y directions.

Fig. 9 The trajectory of the laser beam on the photodetectors as the cantilever is vertically deflected (with no torsional motion) for a misaligned photodetector with respect to the laser beam. For a change of normal force (vertical deflection of the cantilever), the laser beam is projected at a different position on the detector. Due to a misalignment, the projected trajectory of the laser beam on the detector is not parallel with detector vertical axis (the line joining T-B).

Fig. 10 FFM and (FFM_T) signal as a function of cantilever vertical deflection for Si_3N_4 sliding on graphite in x (open circles) and -x (closed circles) directions. The FFM signal is not directly a measure of friction force. Only the half of the differential signal between these two scans (FFM_T , open triangles) is the real friction signal.

Fig. 11 Illustration showing the deflection of cantilever as it is pushed by (a) a rigid sample or by (b) a flexible spring sheet.

Fig. 12 Displacement curve of the cantilever tip as it is pushed towards (extending) and pulled away from (retracting) a silicon sample. The large separation between point B where the tip is touching the sample and point C where the tip is pulled off the sample is due to a large pull-off (adhesive) force between the tip and the sample.

Fig. 13 A typical profile of the PZT height as a Pt sample is scanned back and forth in y and -y directions. The normal load is about 50 nN. The cantilever stiffness is 0.4 N/m.

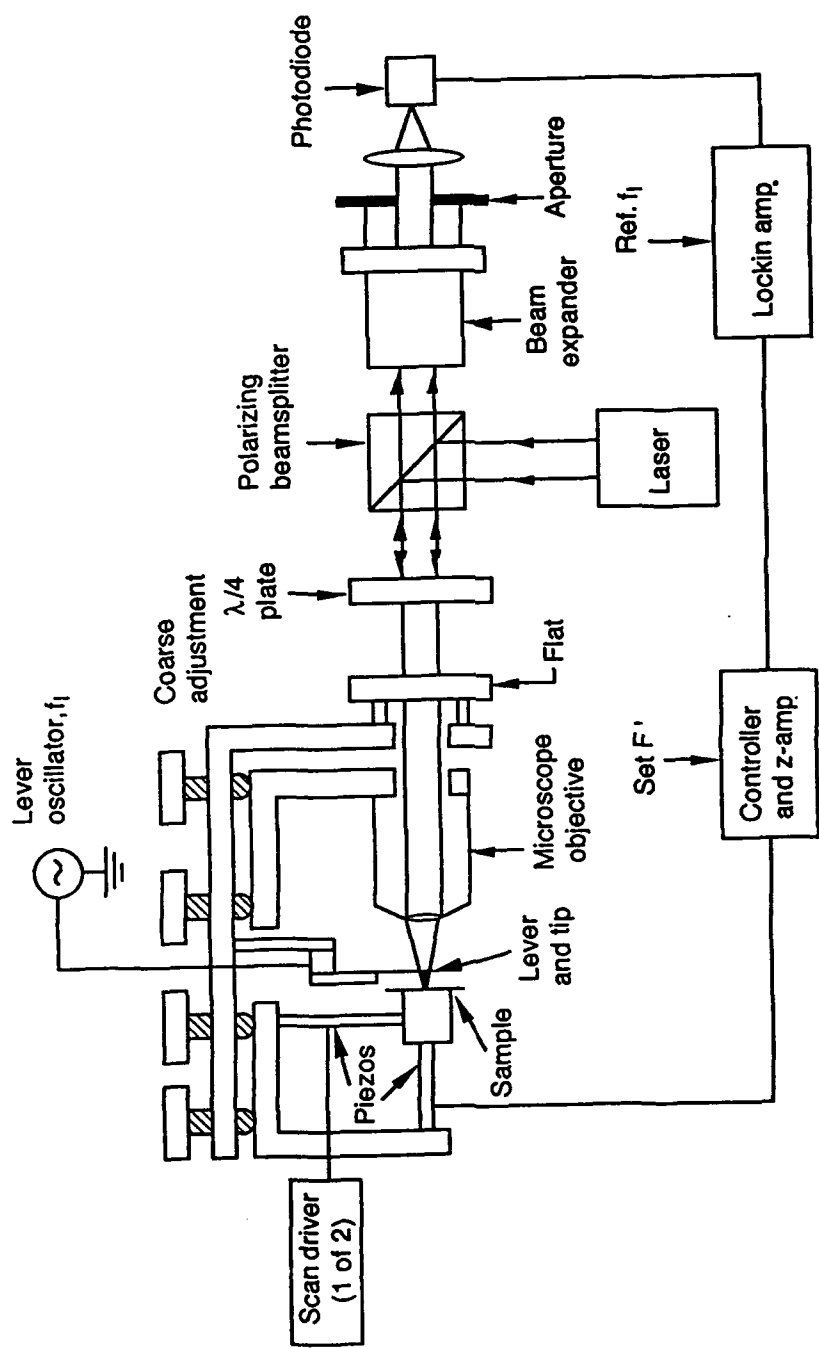
Fig. 14 The vertical height difference (separation of the surface profile, $\Delta H_1 + \Delta H_2$) as a function of the PZT center position (PZT height H_0) between the two traveling directions (y and -y) of a Pt sample. The three symbols represent three sets of repeated measurements. The slope of the linear fit is proportional to the coefficient of friction between the Si_3N_4 tip and Pt.

Fig. 15 Friction signal as a function of cantilever vertical deflection for Pt. Different symbols represent eleven sets of repeated measurements. The slope of the linear fit is proportional to the coefficient of friction between the Si_3N_4 tip and Pt. Vertical cantilever stiffness is 0.4 N/m and the friction signal is 8.6 nN/V.

Fig. 16 Friction force as a function of normal force for Si_3N_4 tip sliding against silicon, diamond, and graphite.

Fig. 17 Schematic showing the beam alignment with the cantilever. A platform containing a laser diode and a prism is tilted to bring the beam to one of the two cantilevers C1 and C2. This results a non-vertical projection of the beam on the levers. Therefore the projection of the reflected beam (PP') on the photodetector as the cantilever is deflected up and down due to a change of normal force is at an angle relative to the vertical axis (CC') of the detector.

Fig. 1



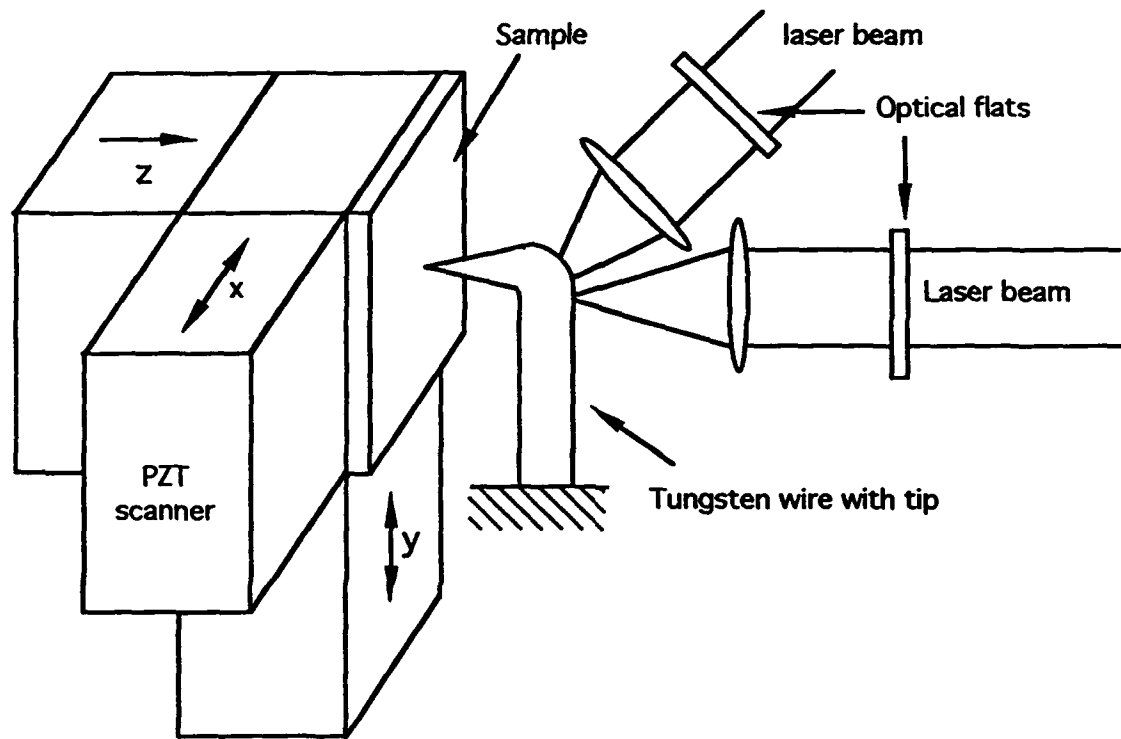


Figure 2

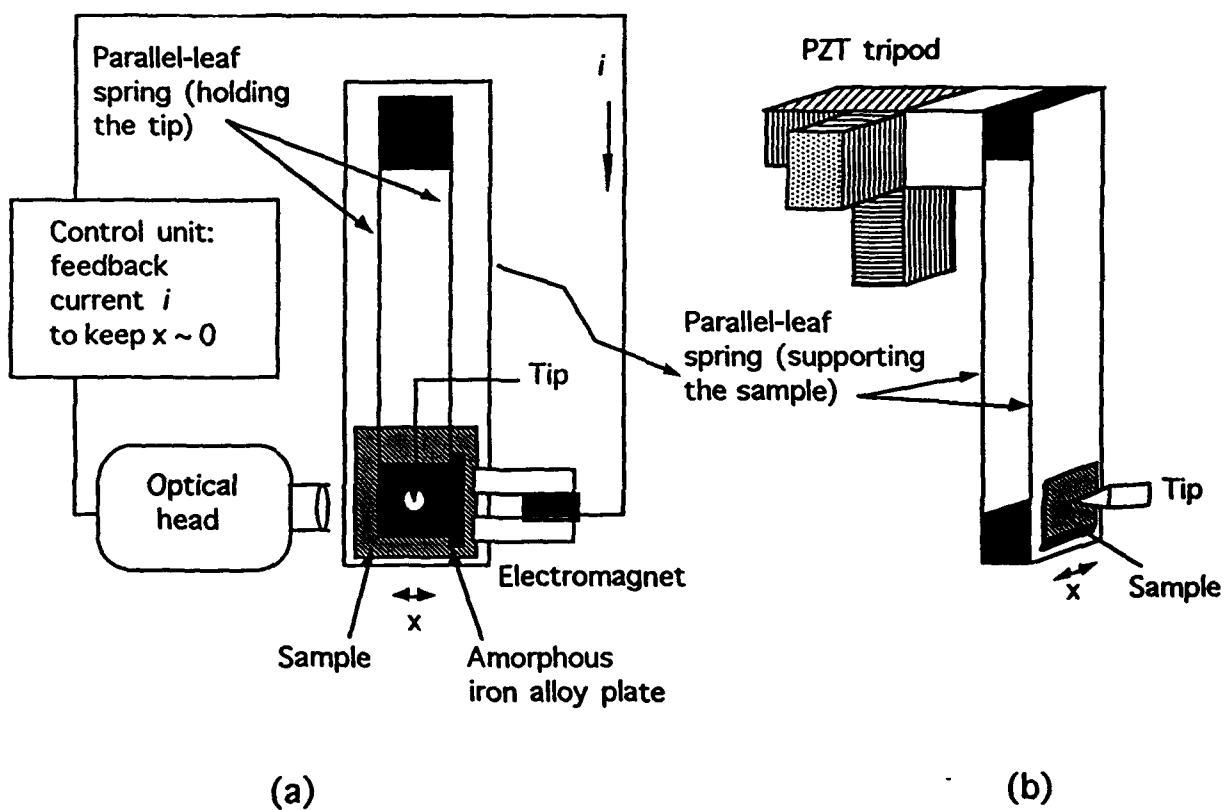


Figure 3

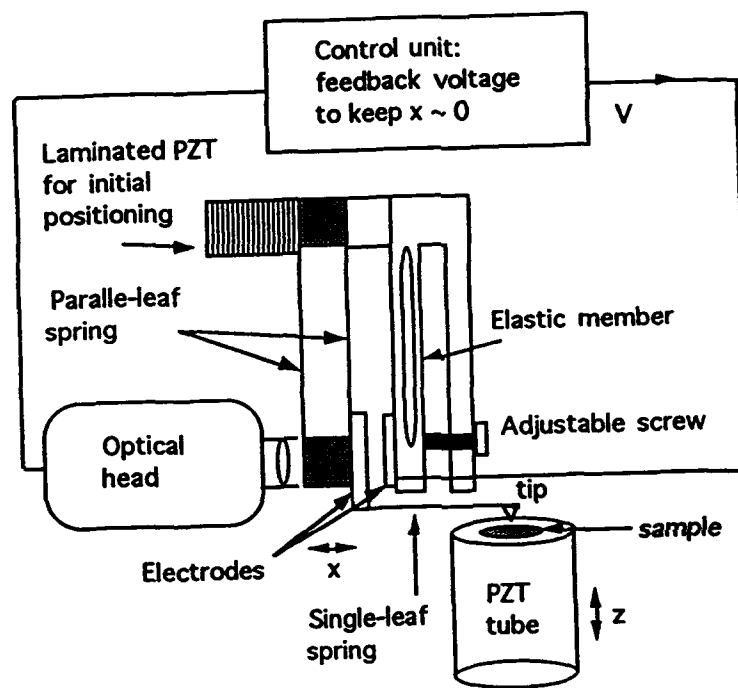


Figure 4

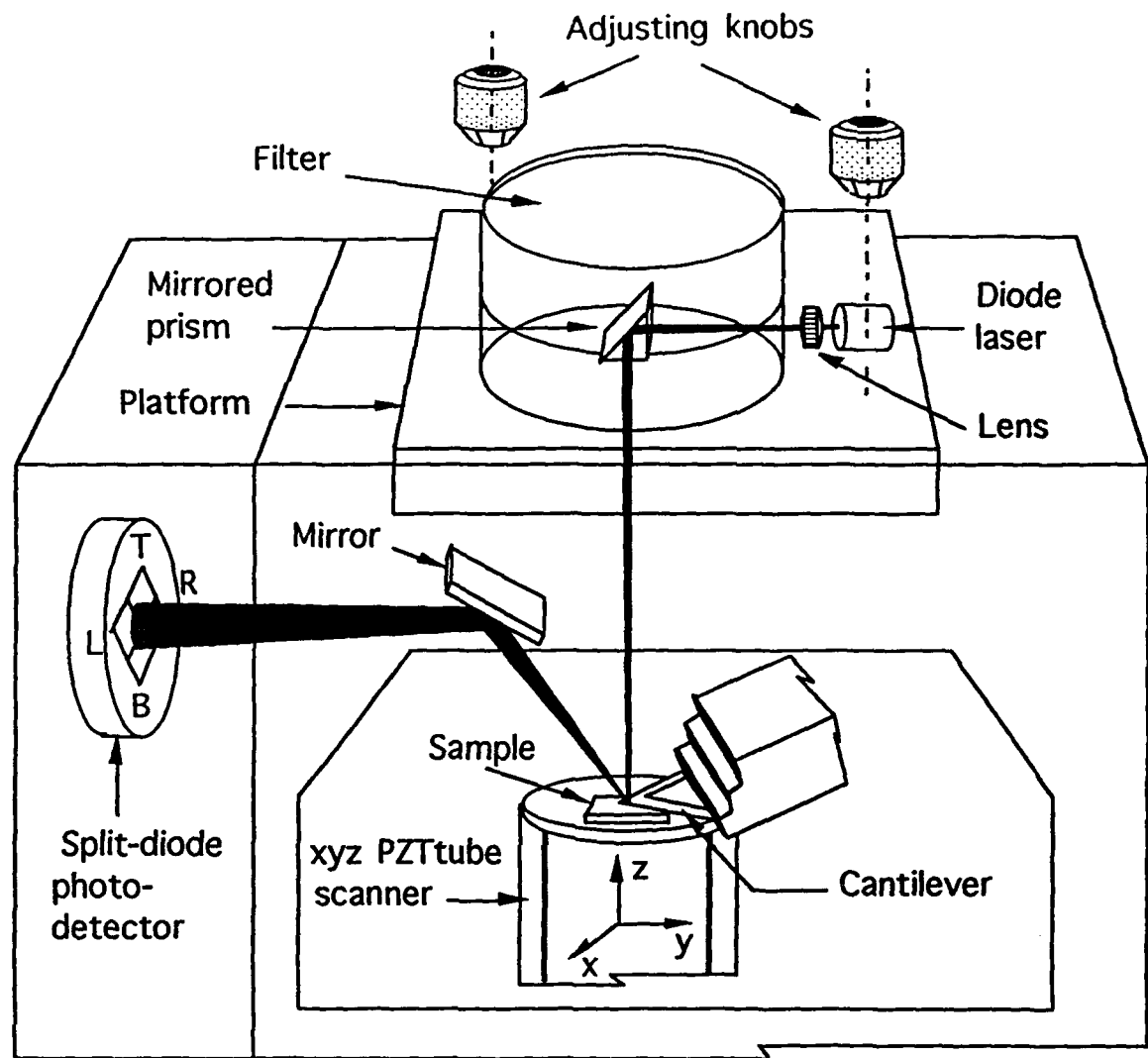


Fig. 5a

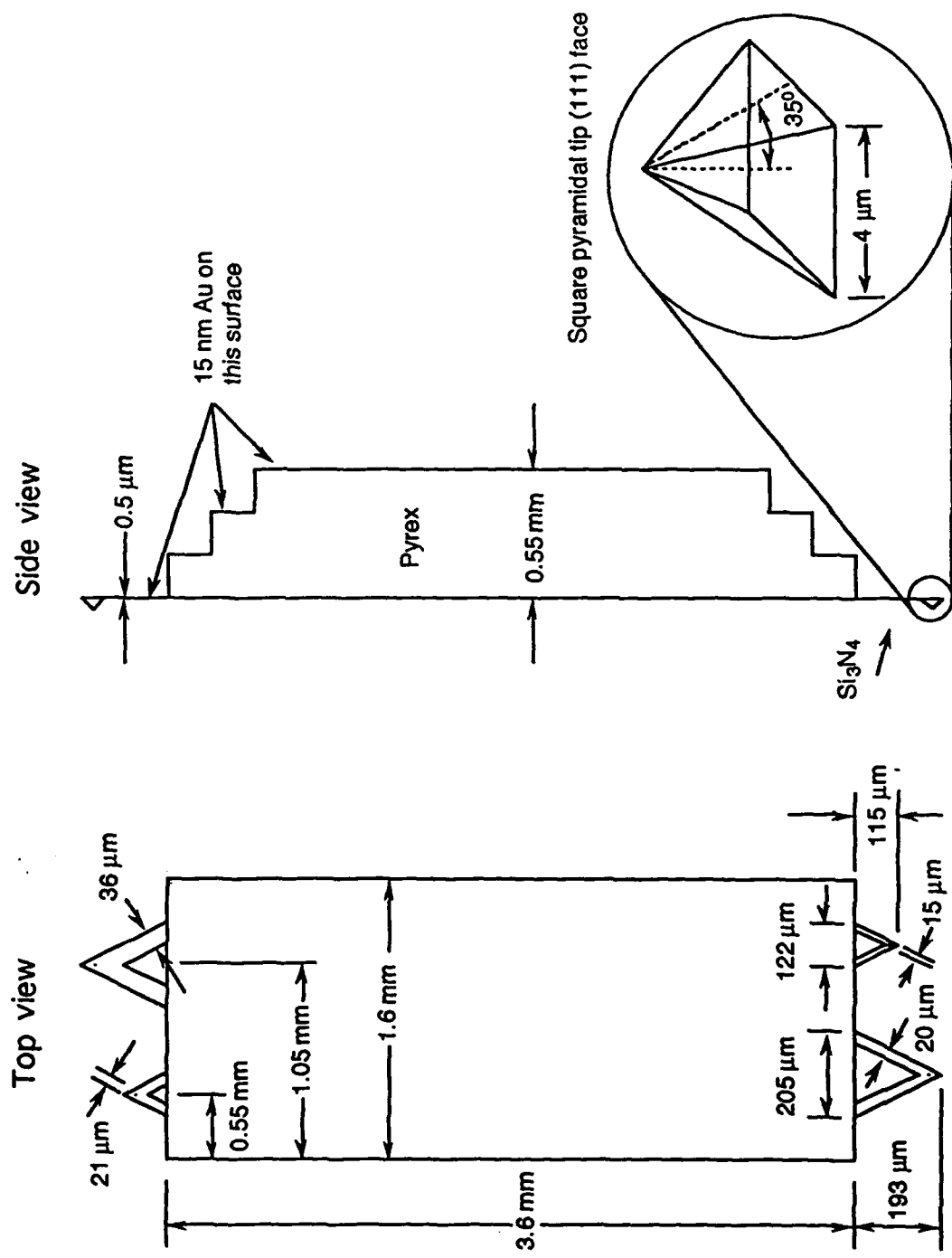
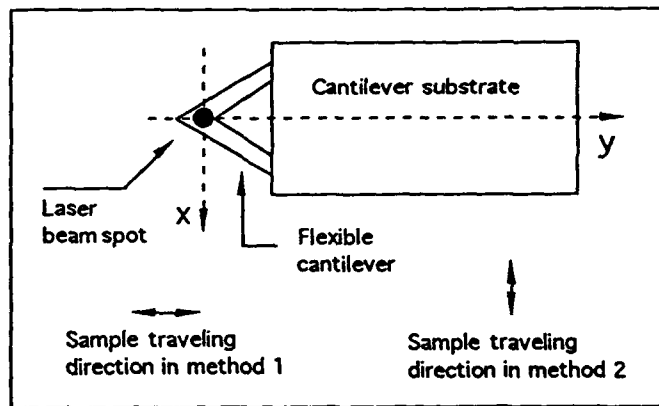
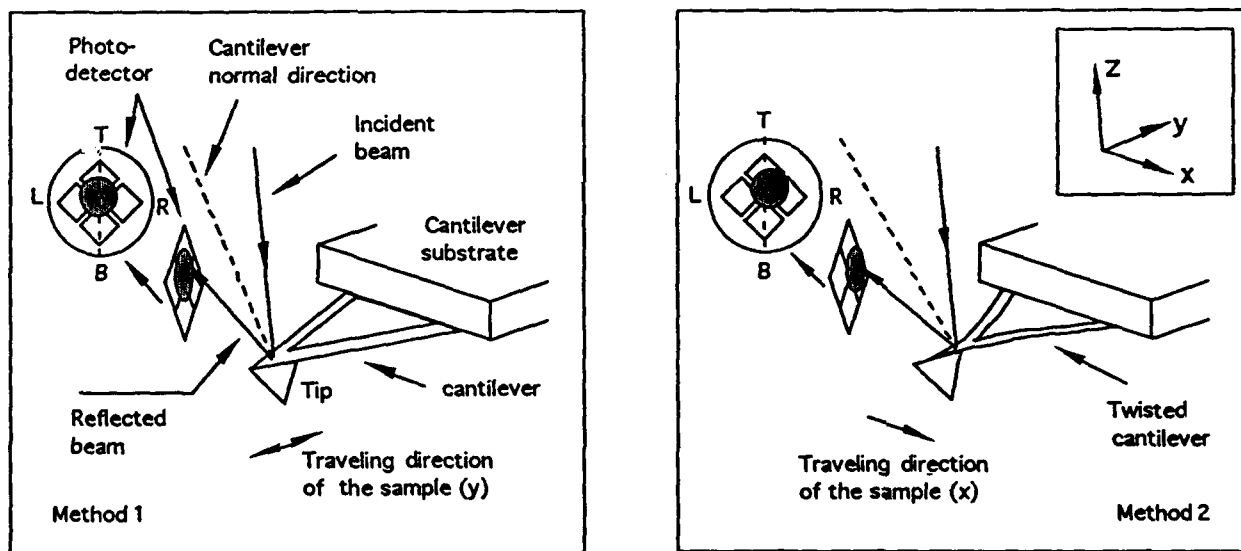


Fig. 5b



(a)



(b)

Figure 6

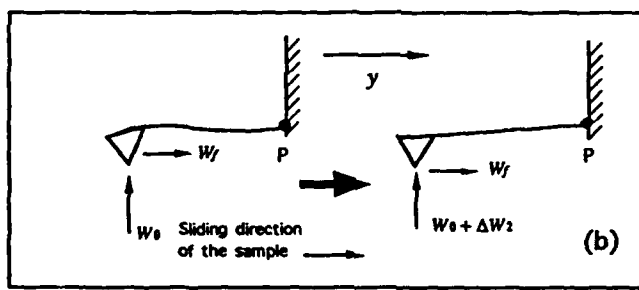
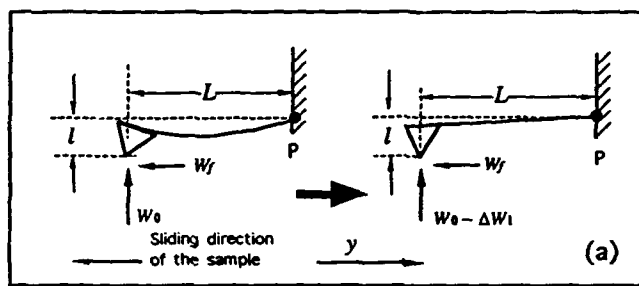


Figure 7

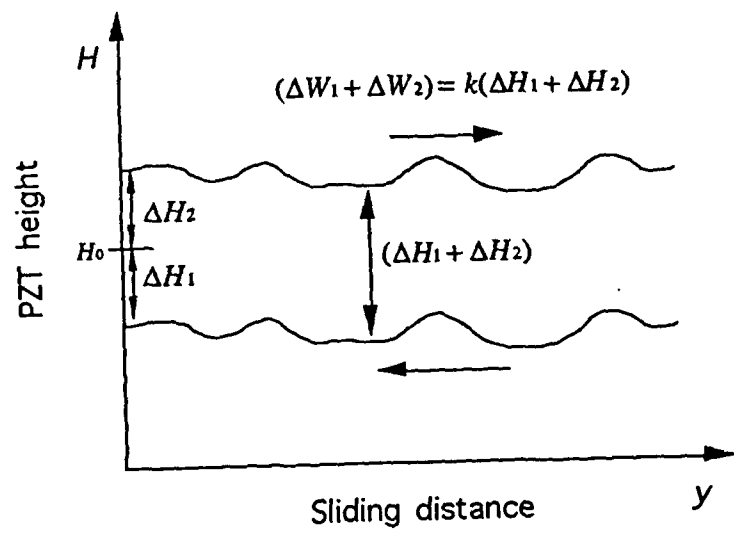


Figure 8

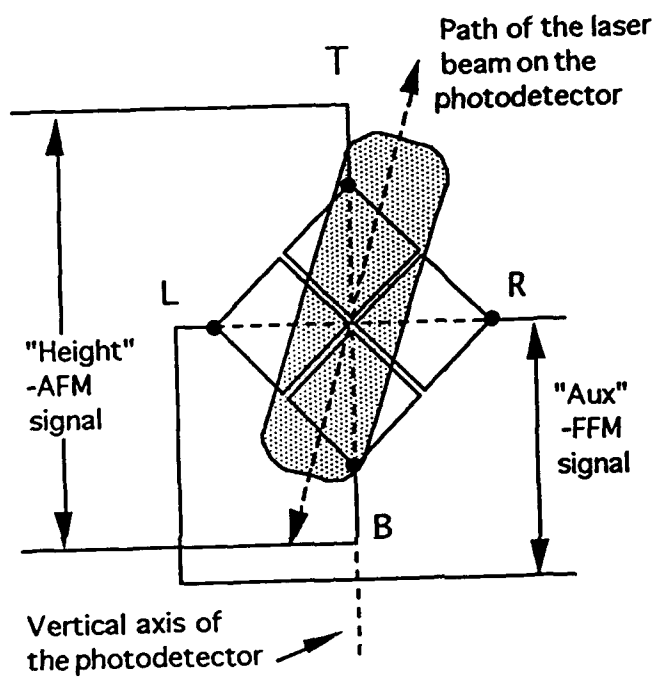


Figure 9

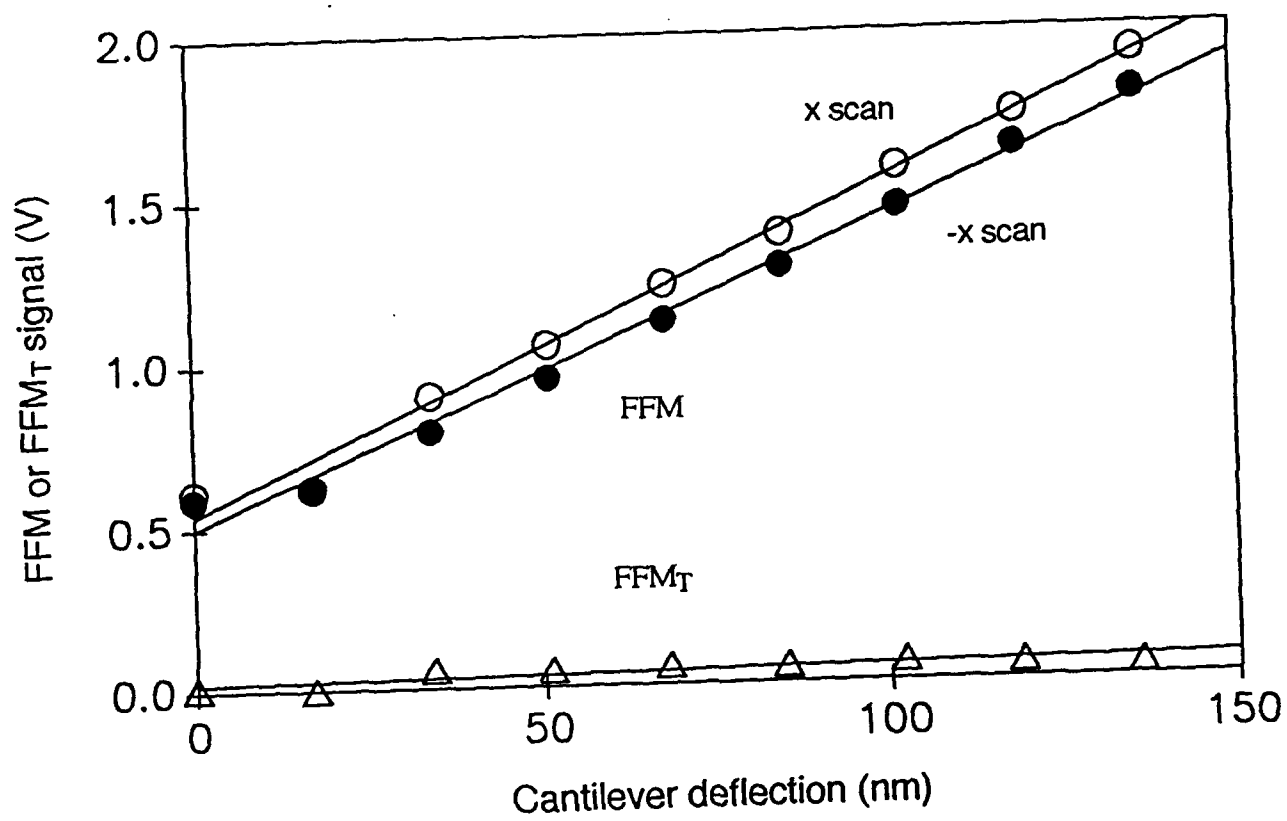
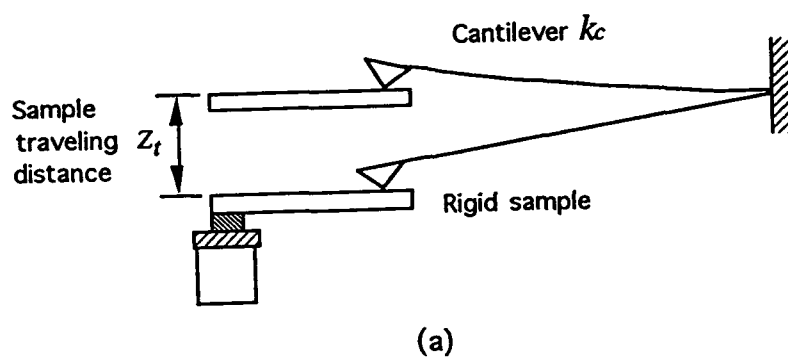
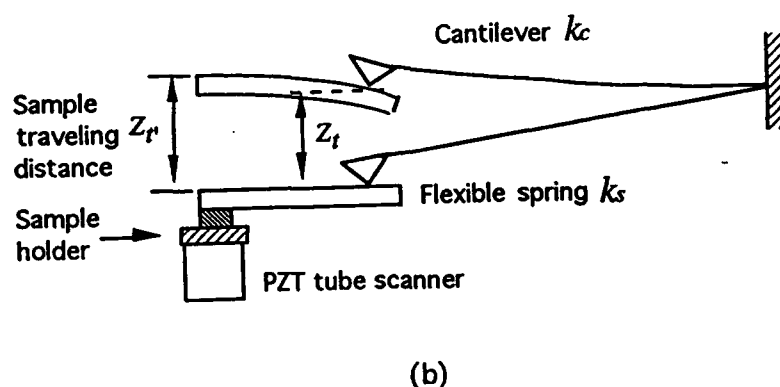


Fig. 10



(a)



(b)

Figure 11

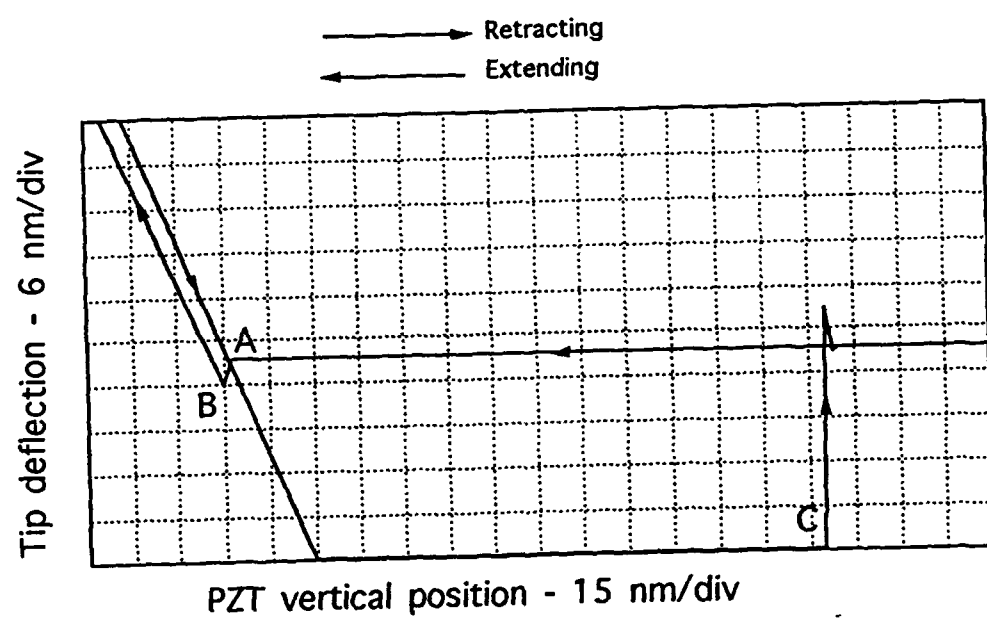


Fig. 12

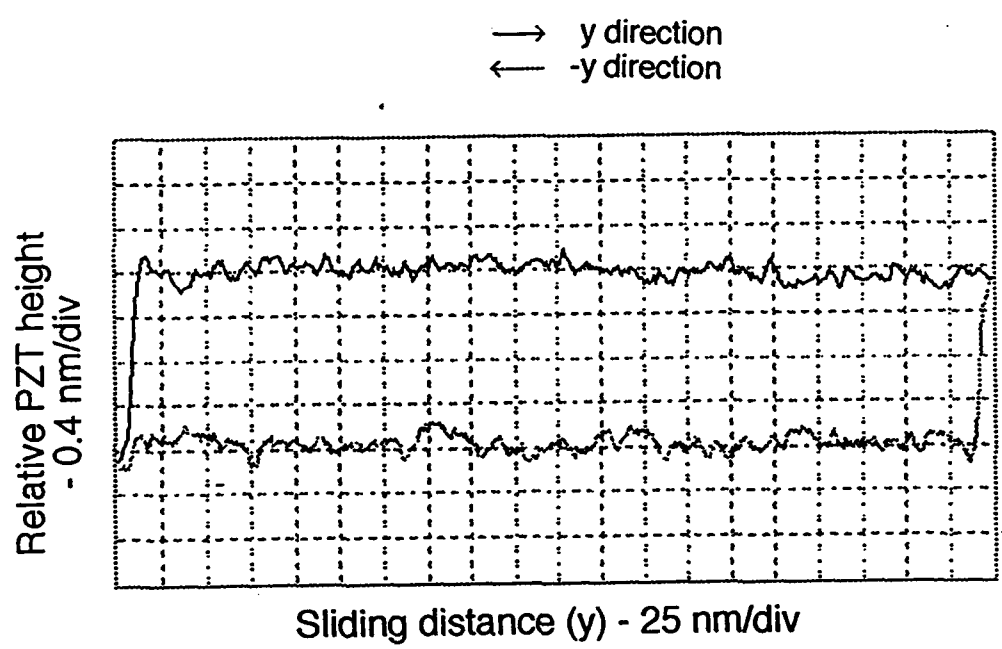


Fig. 13

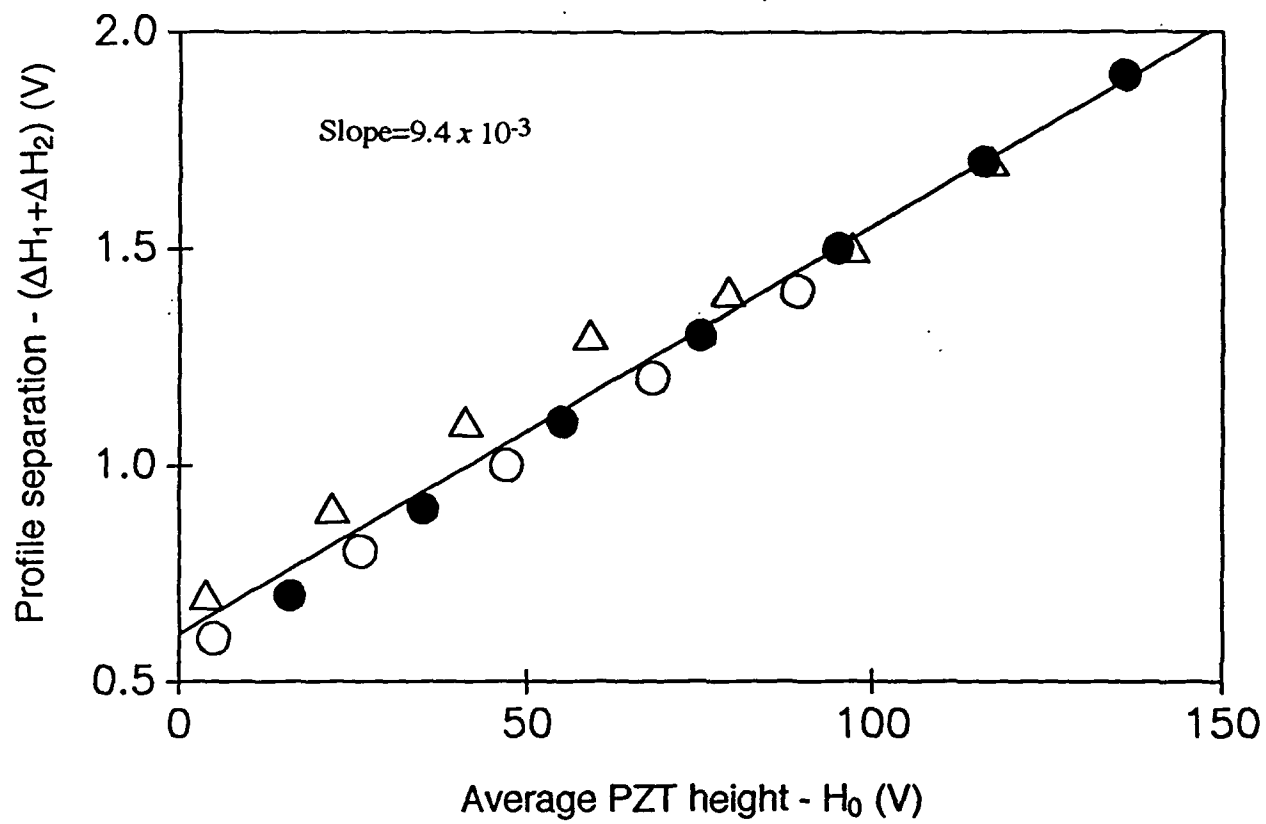


Fig. 14

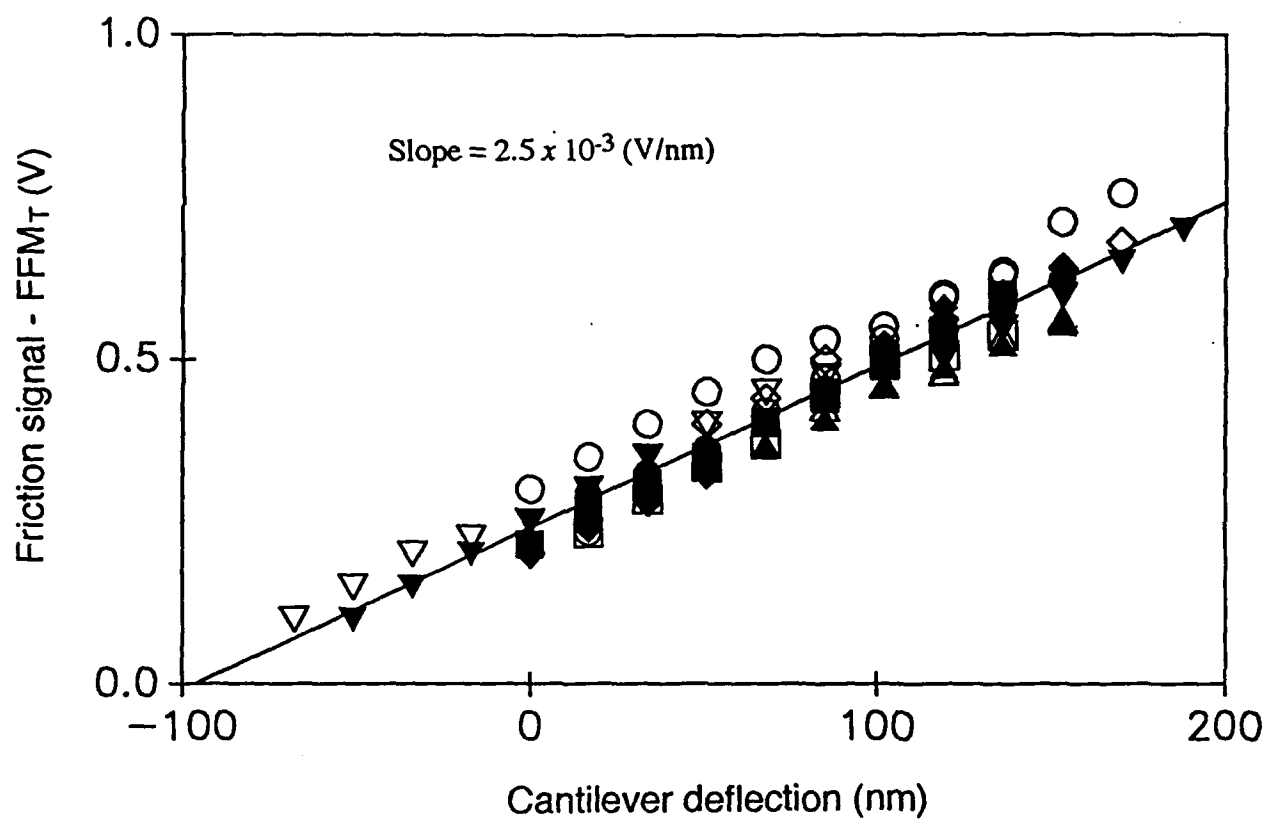


Fig. 15

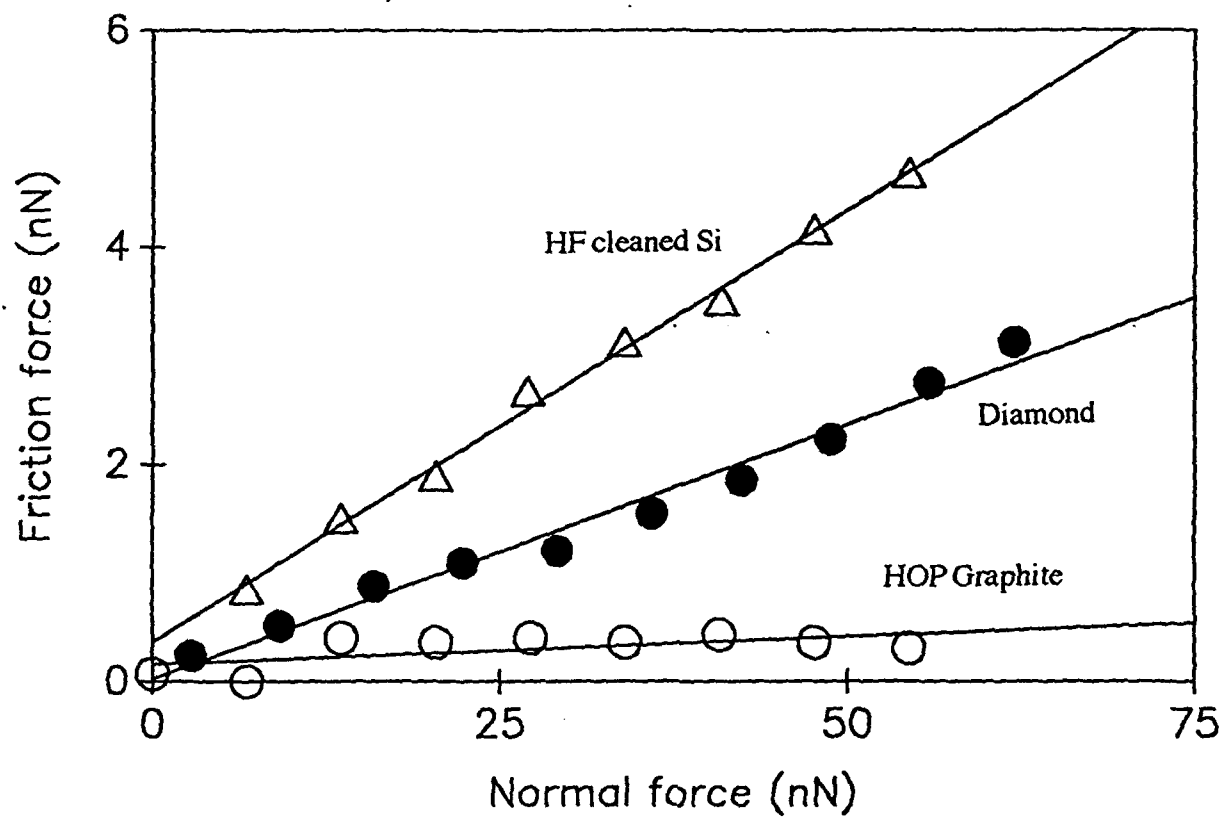


Fig 16

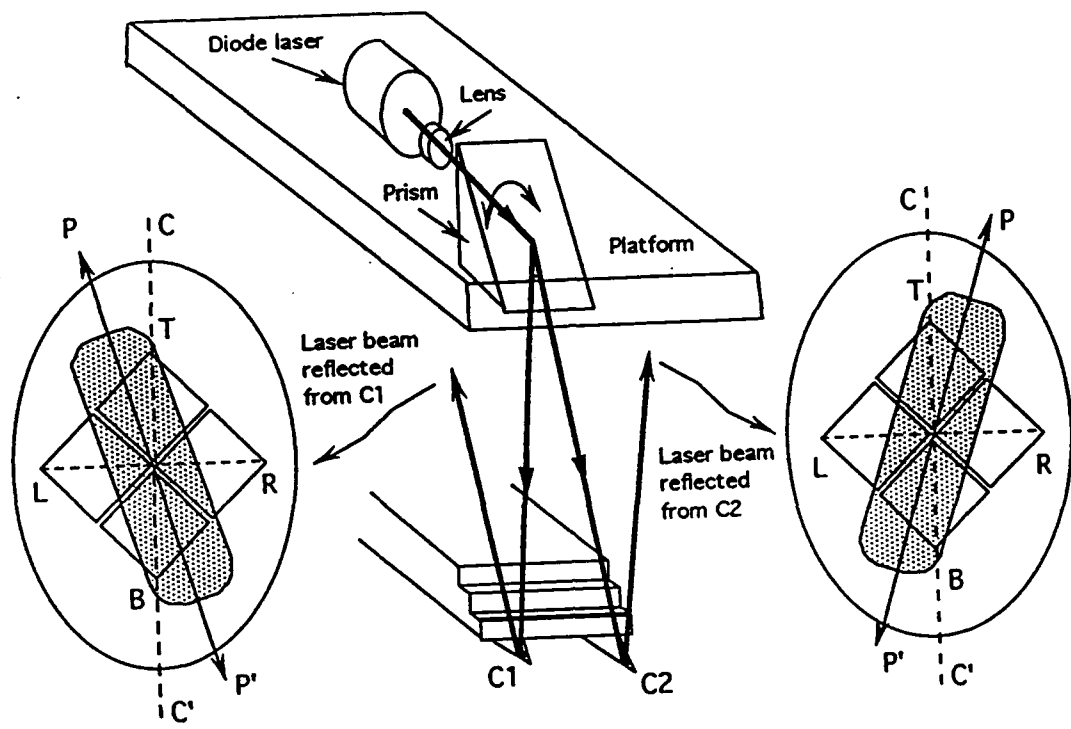


Figure 17